

Microscopic examination of hot spots giving rise to nonlinearity in superconducting resonators

Cihan Kurter,¹ Alexander P. Zhuravel,² Alexey V. Ustinov,³ and Steven M. Anlage¹

¹*Center for Nanophysics and Advanced Materials, Department of Physics,
University of Maryland, College Park, Maryland 20742-4111 USA*

²*B. Verkin Institute for Low Temperature Physics and Engineering,
National Academy of Sciences of Ukraine, 61103 Kharkov, Ukraine*

³*Physikalisches Institut and DFG-Center for Functional Nanostructures (CFN),
Karlsruhe Institute of Technology, D-76128 Karlsruhe, Germany*

(Dated: September 14, 2011)

We investigate the microscopic origins of nonlinear radio frequency (*RF*) response in superconducting electromagnetic resonators. Strong non-linearity appearing in the transmission spectra at high input powers manifests itself through the emergence of jump-like features near the resonant frequency which evolve towards lower quality-factor with higher insertion loss as *RF* input power is increased. We directly relate these characteristics to the dynamics of localized normal regions (hot spots) caused by microscopic features in the superconducting material making up the resonator. A clear observation of hot spot formation inside a Nb thin film self-resonant structure is presented by employing the microwave laser scanning microscope, and a direct link between microscopic and macroscopic manifestations of nonlinearity is established.

PACS numbers: 74.81.-g, 74.25.N-, 74.62.Dh

I. INTRODUCTION

Microwave resonators utilizing superconducting thin films have enabled development of various nonlinear devices including bifurcation amplifiers¹, hot electron mixers², and kinetic inductance photon detectors^{3,4} among other examples. They have been crucial elements in circuits designed for quantum computation⁵. Recently, these on-chip resonators have started to appear in meta-material designs promising new possibilities such as negative refractive index⁶, electromagnetically induced transparency⁷, tunable THz response⁸, and parametric amplification of negative index photons⁹.

Nonlinearity is manifested in many forms, including a reduction in quality factor, an increase in insertion loss, shift of the resonant frequency¹⁰, or appearance of abrupt jumps in the transmission/reflection characteristics¹¹. Understanding the microscopic origin of such a response is essential. Various mechanisms have been proposed to explain the nonlinear characteristics at elevated microwave power, including both intrinsic and extrinsic types. Among them, hot spot formation is found to be one of the major mechanisms, which was both theoretically and experimentally studied in superconducting strip conductors and resonators¹².

A clear and compelling connection between the microscopic models and the macroscopic picture of nonlinearity revealed by microwave measurements is still lacking. Here we establish this connection through a study of the radio frequency (*RF*) response of a two-dimensional spiral resonator made up of 200 nm Nb thin film on a quartz substrate via the Laser Scanning Microscopy (*LSM*) technique.

II. EXPERIMENT

The resonant structures have been designed as engineered *meta-atoms* (planar spirals) of *RF* metamaterials intended to create a strong magnetic response in the sub-100 MHz range^{13,14}. Prior results show that the spirals act as very compact self-resonant structures, supporting up to 10 half-wavelength standing waves of *RF* current¹⁴. The *free space* stimulation of these spiral resonators is done by sandwiching them between two *RF* antennas made up of loop-terminated coaxial cables whose other ends are connected to an *RF* network analyzer. Exciting the spirals results in Lorentzian type resonant peaks in transmission for low levels of *RF* stimulus power¹⁴. The peaks do not change in shape or position over a broad range of input powers. When the spirals are strongly driven, the resonant characteristics begin to develop notches near the center of the transmission peaks¹¹. Those nonlinear features evolve with *RF* power and are believed to be associated with the existence of non superconducting regions in the Nb thin films causing resistive *hot spot* formation.

The high-power properties of superconducting strip resonators are very sensitive to the geometrical structure of the current-carrying conductors¹⁵. Our continuous circular spirals have a unique geometry (see the left inset of Fig. 1) in which the currents flowing in neighboring turns are parallel, and approximately equal in magnitude, at least for the first few resonant modes, in contrast with the current flow profile in meander-line resonators used for photon counting⁴. In the spiral, the magnetic fields generated by flowing currents largely cancel in the region between the strips, leading to a self-field pattern nearly parallel to the plane of the spiral. This geometrical effect greatly reduces the accumulation of *RF* currents at

the edges of the strip. Moreover, the continuous arc of the spiral allows for a relatively homogenous and uniform flow along the windings compared to sharp-cornered structures that have a tendency to pile up the currents at the corners and edges^{16,17}.

III. RESULTS AND DISCUSSION

A. Global Microwave Transmission Measurements

The main panel of Fig. 1 shows the global microwave transmission response of a Nb spiral resonator for a set of RF input powers at 4.4 K. The spiral has an outer diameter, D_o of 6 mm and 40 turns; the strip width, w and spacing, s between the turns are $10\ \mu\text{m}$. The fundamental resonance gives a pronounced transmission peak at ~ 75.84 MHz for low and moderate RF powers (see Fig. 2 in Ref.¹³). Up to -2 dBm, the resonant peaks almost overlap, i.e., transmission, $|S_{21}(f)|$ is a Lorentzian function of frequency and does not show any significant difference in shape with increasing power (black curves in the right inset). Those curves falling into the linear response regime correspond to a state where Nb is in the hotspot-free superconducting phase. At a critical input power (-1.5 dBm in this case), $|S_{21}(f)|$ makes a sharp transition from one Lorentzian curve onto another with higher insertion loss and lower quality factor, Q , as frequency is scanned near resonance (the highest red curve in the right inset).

As the driving frequency is swept from lower values towards the resonance frequency, f_0 , the circulating RF power builds up in the resonator and the circulating currents I_{circ} in the spiral will increase in magnitude, as $I_{circ} = I_{max} / \sqrt{1 + [(f - f_0)/\delta f]^2}$ where I_{max} is the maximum current induced in the resonator and δf is the 3 dB bandwidth. For low/medium RF input powers, no instantaneous power value causes excess dissipation because even the maximum current at resonance is low enough to maintain the linear characteristics. For the high input power case, the cavity is over-driven in the vicinity of f_0 and thermal effects cause the breakdown of superconductivity. The over-stimulation of the resonator launches a new dissipation mechanism and the resonant response moves onto a different curve with lower Q corresponding to initial stages of a hot spot. With increasing input power this transition occurs at progressively lower frequencies where the dissipative mechanism is activated (the red curves in the right inset of Fig. 1). At still higher powers, a second discrete dissipative mechanism is activated, leading to another set of discontinuous curves (blue curves). At even more elevated powers one has either a large number of discrete dissipation centers activated, or an expansion of the original hot spots, giving rise to a flattening of the transmission spectrum (orange curves), and eventually to a dip or crater (brown curves).

The f_0 of the Nb spiral remains roughly constant with increasing power, unlike what is seen in temperature de-

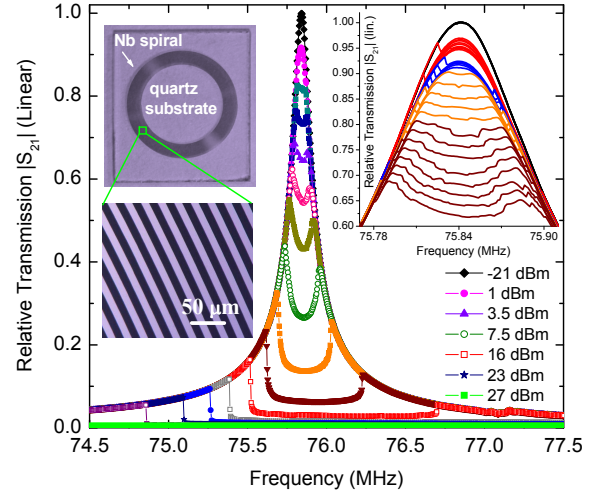


FIG. 1: (Color online) Global microwave transmission response from a $D_o = 6$ mm spiral with 40 turns and $w = s = 10\ \mu\text{m}$ for a set of RF input powers at $T = 4.4$ K. Right inset: A closer look at the linear and nonlinear regimes evolving with increasing input power. Black Lorentzian type curves corresponding to power values from -21 dBm to -2 dBm overlap, progressively evolving into the red curves for power values between -1.5 dBm and +0.6 dBm then blue curves for powers from +0.7 to +1.1 dBm, orange curves from +1.2 dBm to +2 dBm and brown curves from +2.2 dBm to +3.6 dBm. Top Left inset: An optical image of a spiral resonator with $D_o = 6$ mm and 40 turns. Bottom Left inset: Zoom in the area marked in the top left inset showing the Nb spiral windings in detail. Dark strips are Nb turns in the picture.

pendence data where the resonance shifts to smaller frequencies⁷. At the extreme case of input power, the dissipation is so large that superconductivity is quenched and the entire resonant feature is wiped away from the spectrum (see the data at +27 dBm). Note that upon reducing the power the resonant features are re-established.

B. Laser Scanning Microscopy

To develop a microscopic understanding of the nonlinear resonant features in the transmission data, we examined the spiral resonators with the *LSM* technique^{17,18}. For these measurements, the Nb spiral is stimulated by RF signals well below its transition temperature, T_c and is scanned by a focused laser probe. The spiral resonator is supported on a sapphire disk along with a thermometer and heater located on a metallic platform nearby, inside an optical cryostat. The RF excitation has been done by two RF loops in a manner identical to that described above. A diode laser beam of 5 mW power and a wavelength of 645 nm illuminates the spiral surface. For the large-scale *LSM* images (up to $10 \times 10\ \text{mm}^2$ scanned area with 500×500 points), a collimated laser beam is focused onto a spot with a diameter of $20\ \mu\text{m}$ that produces an estimated temperature difference, δT of 1.2 K at most

relative to an area on the sample unexposed to the laser beam. For more detailed examination of the spiral surface (within a maximum scanned area of $250 \times 250 \mu\text{m}^2$), a $1.6 \mu\text{m}$ diameter laser beam is used. The raster scanning of the spot is done with $0.2 \mu\text{m}$ steps, much smaller than the laser spot diameter. However, the amplitude of the laser is modulated at a frequency of 100 kHz, which is significantly smaller than the inverse phonon escape time (on the order of nanoseconds), thus creating a steady state temperature profile¹⁸. Moreover, the beam intensity is reduced by neutral-density optical filters down to 1 mW/mm^2 , so the temperature rise is reduced to $\delta T = 0.1 \text{ K}$.

The *LSM* technique basically images photoresponse (*PR*) which comes from the changes induced by periodically modulated laser power in the transmission characteristics ($\sim(\partial|S_{21}(f)|/\partial T)\delta T$) of the spiral, synchronously detected with a lock-in amplifier. The response can be decomposed into inductive and resistive components¹⁷. Since the temperature is well below the T_c of Nb for the measurements shown here, the modulation of penetration depth λ (thus the inductive response) is small, so the contrast in the *LSM* images is mainly due to resistive *PR*, which is proportional to $\delta(\int R_s \lambda^2 J_{RF}^2(x, y) dS)$, where the integral is carried out over the area of laser-induced perturbation. The *PR* is therefore a convolution of changes in resistance below T_c , δR_s , weighted by the local value of *RF* current density squared, $J_{RF}^2(x, y)$.

Large-scale ($7 \times 7 \text{ mm}^2$), low temperature (4.8 K) *LSM* images of the Nb spiral presented in Fig. 1 are shown in Fig. 2(a) and (b). The excitation of the spiral is done at the fundamental frequency of $\sim 73.6 \text{ MHz}$ ¹⁹ at which the first emerging hot spot is detected at +10 dBm (a). By the time the power is ramped up to +20 dBm, the entire sample is heated and the resistive response allows imaging of a convolution of δR_s and the current distribution in the entire spiral (b), showing a single half-wavelength of standing wave current spanning the length of the spiral. Most of the *PR* comes from the middle windings, and diminishes near the inner and outer edges¹⁴. The brighter areas observed on the left side and the lower half of the spiral in (b) are caused by the structural/morphological defects with enhanced δR_s .

The upper half of the spiral is free of physical imperfections (no defect is visible with $0.5 \mu\text{m}$ resolution reflected light microscope), thus we have concentrated on a small portion of that area to examine the appearance of the first microscopic defect. Figs. 2(c)-(f) are a detailed examination of the $30 \times 30 \mu\text{m}^2$ area on the Nb spiral marked in (a) and show the evolution of the first hot spot with increasing *RF* power at 4.8 K. At +10 dBm, we observe two bright spots in their initial phase at the opposite edges of a single strip in the spiral (c), reminiscent of vortex-antivortex formation at the edges of the current carrying superconducting stripes²⁰. As the power is increased, the isolated spots expand and start to merge together (d) where presumably phase-slip lines

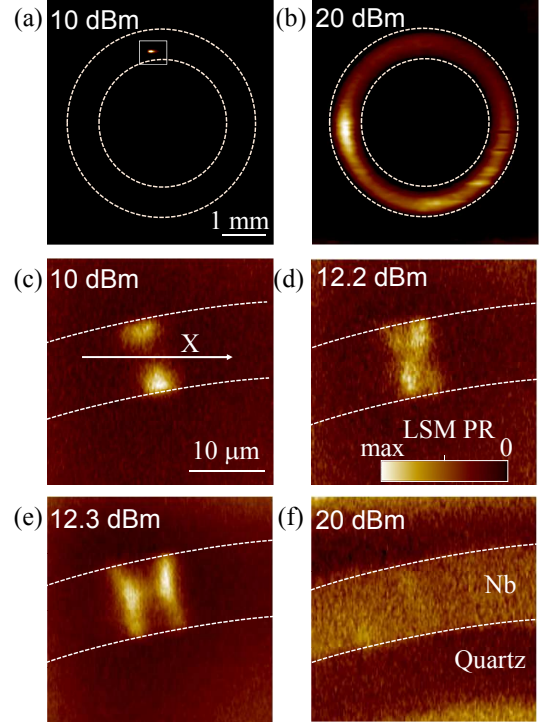


FIG. 2: (Color online) *LSM PR* images of the nucleation and RF power evolution of a hot spot. (a) Detection of the first microscopic defect causing the hot spot formation on the Nb spiral resonator whose details are discussed in Fig. 1 at +10 dBm, 4.8 K. (b) The hot spot shown in (a) heats the neighboring area and creates a resistive response coming from the entire spiral at +20 dBm. The length scale bar in (a) is the same for (b). (c)-(f) Zoom in of the $30 \times 30 \mu\text{m}^2$ area marked in (a) at progressively higher input powers. The color-scale bar in (d) applies to all *LSM PR* images shown in Fig. 2, the maximum *LSM PR* corresponds to 0.3346 mV for (a), 0.1857 mV for (b), 3.6 μV for (c), 11.4 μV for (d), 23.2 μV for (e) and 12.4 μV for (f). The length scale bar in (c) applies to the images in (c)-(f).

(i.e. isothermal nonequilibrium regions)²¹ are formed. Further increase in *RF* power causes a change of the arrangement of these phase-slip lines (e) due to the redistribution of current flow along the strip. This follows from the nucleation of a normal domain across the strip interfacing with resistive superconducting domains [the bright regions established along the wings of a butterfly pattern seen in (e)]²². With even further increase in power the normal domain expands along the strip and finally, the entire strip shows a resistive response (f).

The formation of a phase-slip line in the *DC* resistive state is signaled by the emergence of step-like features in the $I(V)$ characteristics. Although the phase-slip lines discussed in this paper are generated by the combination of *RF* excitation and laser power, we see a very similar picture. The data presented in Fig. 1 with gradually degrading Q-factor with increasing *RF* input power make a good analogy to the characteristics of the *DC* bias case

with changing differential resistance as the voltage is increased.

We further studied the structure of the hot spot with another sub-100 MHz Nb spiral at 4.5 K. The spiral examined in Fig. 3 has 45 turns, $D_o = 5$ mm and $w = s = 10$ μm . Here, the laser beam passes through the hot spot on a 20 μm line scan [shown with 'X' in Fig. 2(c)]. The frequency is swept through resonance ($f_0 \sim 88.2$ MHz) along the X-line cut, to create a position vs. frequency image of the hot spot at a fixed RF input power. Figs. 3(a)-(d) show RF power evolution of the hot spot within a 20 μm line as frequency is scanned in a narrow band centered on f_0 , while the corresponding PR profiles at a fixed position, x_0 near the center of the hot spot are shown in (e)-(h) for both directions of frequency sweep. At 0 dBm, in the initial stages of the hot spot, one sees a strong Lorentzian $PR(f, x_0)$ along with a linear $|S_{21}(f)|^2$ [(a) and (e)], reminiscent of that at low power shown in Fig. 1. In the case of a spatially invariant δR_s , the dissipative term of $PR(f)$ originates from the temperature dependence of $J_{RF}^2(f)R_s(T)$, meaning that it can be described by a simple difference between two $|S_{21}(f)|$ characteristics $\delta|S_{21}(f)| \sim J_{RF}^2(f)[R_s(T_2) - R_s(T_1)]$, where T_1 is the temperature of the non-radiated area while T_2 is the temperature of the area radiated by the laser probe on the Nb film. At low RF powers, the temperature effect of the laser on transmission will be small, hence the PR traces out a Lorentzian-like curve, as seen in (e).

As the power increases, the hot-spot produces a non-linear behavior of $\delta R_s(J_{RF}, T)$ causing peculiar jumps in $|S_{21}(f)|$ whose trend is mimicked by $PR(f)$. At +4 dBm [(b) and (f)], in the middle of the hot spot, one first sees a Lorentzian-like response at the onset of the frequency sweep, but then a *breakdown* occurs at a critical frequency, and a *crater* develops in the $PR(f)$ trace similar to that seen in the higher power $|S_{21}(f)|$ characteristics in Fig. 1. Note that these line cuts are not hysteretic; i. e. forward (blue curves) or backward (red curves) sweep of the frequency reproduce the same characteristics.

An important question arises: why does the LSM PR drop in the crater? Is it due to a decrease in δR_s or J_{RF} , or both? In fact, both mechanisms should contribute since LSM $PR \sim (\partial R_s / \partial T)(\delta T) + (\partial J_{RF} / \partial T)(\delta T)$. The dissipative component of LSM PR is proportional to both δR_s and changes in the normal (non-superconducting) component of J_{RF} , δJ_{RF} . The latter is reduced in the resistive state due to the diminished superfluid density. In this case, a crater-like pattern is formed due to time averaging of LSM PR coming from the localized regions where resistive superconducting and normal domains are side by side, as in phase-slip processes^{21,23}. When a fully normal domain is formed, $\delta R_s \sim \delta R_N$, where δR_N is the very small change in normal state resistance with temperature, thus the LSM PR drops significantly, as seen in (g).

A higher input power (+5 dBm) LSM imaging of the same x-line scan is shown in (c). Note that there are

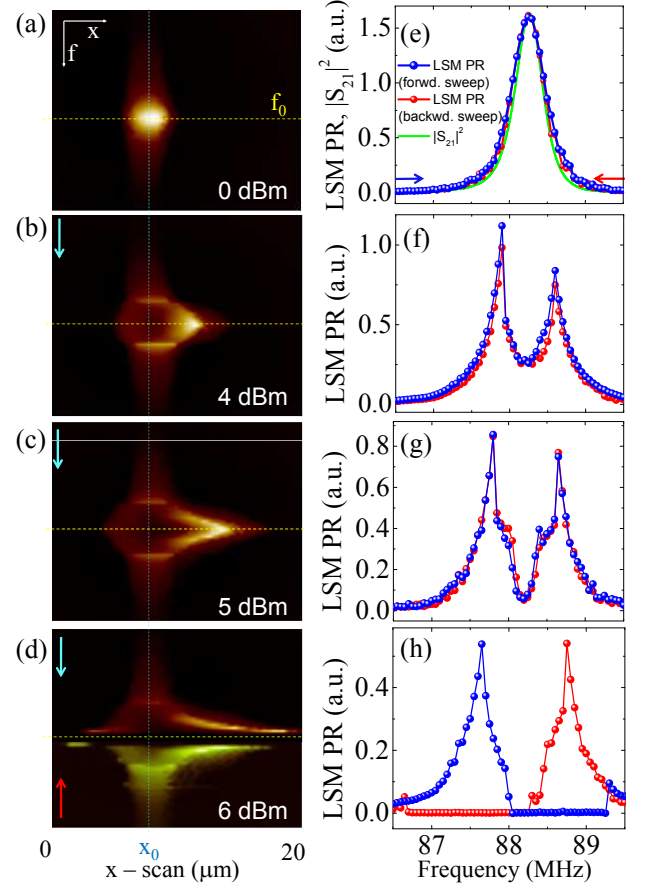


FIG. 3: (Color online) Frequency and space dependence of LSM PR at (a) 0 dBm, (b) +4 dBm, (c) +5 dBm (d) +6 dBm on a Nb spiral with $D_o = 5$ mm, 45 turns, $w = s = 10$ μm over a 20 μm x -scan. The frequency is swept between 86.5 and 89.5 MHz through the fundamental resonant frequency, $f_0 = 88.2$ MHz. The images in (a)-(c) show only forward frequency sweeps whose direction is indicated with blue arrows. In (d), different shade color-maps point out both direction sweeps, shown with blue (forward) and red (backward) arrows. Corresponding $PR(f, x)$ profiles at a fixed position, $x = x_0$ of the laser probe are shown in (e)-(h). The blue dots are the data collected through forward frequency sweep whereas the red dots are those through backward sweep. The $|S_{21}(f)|^2$ at low power, 0 dBm is shown in (e). The color-scale bar in Fig. 2(d) applies to all LSM images shown in Fig. 3 as well, the maximum LSM PR corresponds to (forward/back sweep)-(1.61/1.62) mV for (a); (1.49/1.5) mV for (b); (1.54/1.55) mV for (c); and (1.12/1.4) mV for (d).

now two shoulders and a central valley at resonance in the PR profile shown in (g). Our interpretation is that there is a RF critical (still partially superconducting) state with significant δR_s for excitation frequencies on the shoulders. In the PR valley, the material has become normal, mimicking what we have observed in Fig. 2(e).

With more power, at +6 dBm, the central valley at resonance becomes deeper (d) and at some point the PR drops to zero (h). Though away from the resonance some

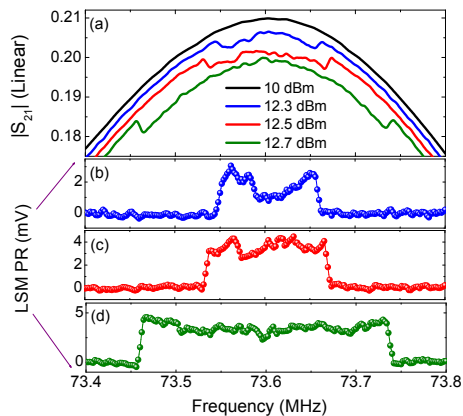


FIG. 4: (Color online) Evolution of global transmission with small increments in RF input power (a), Corresponding *LSM PR* averaged over 100 μm line scans across the center of a *hotspot*. Note that $|S_{21}(f)|$ is measured simultaneously with *LSM PR*(f) when frequency is changed very slowly. A nearly exact correlation between $|S_{21}(f)|$ and *PR* data is evident.

recovery is observed, heating is so significant that back and forth sweeps of frequency can not reproduce the same *PR* profile. Note the hysteresis in (h); the direction of the frequency scan is indicated by blue and red arrows. The size of the resistive domain expands along the x-axis gradually with increasing power and reaches its maximum at +6 dBm (d).

Line cuts at different x locations in Fig. 3 show a continuous variation of *LSM PR*(f) from Lorentzian-like, to flat-top, to cratered, which follows what is seen in the global $|S_{21}(f)|$ measurements shown in Fig. 1. These data provide very clear observation of such a unique connection between local temperature change and global *RF*-power dependent properties of a superconducting resonant system.

To further support the claims made above, Fig. 4 shows the evolution of global $|S_{21}(f)|$ characteristics (a) and

averaged 100 μm line scans of *LSM PR* (b)-(d) with increasing power at 4.5 K, on a 40-turn, $D_o = 6$ mm spiral. The linear $|S_{21}(f)|$ characteristics occurring at +10 dBm [black curve in (a)] turns into nonlinear curves with small increments in *RF* power. The curves are shifted with equal offset in the vertical direction for clarity. With increasing input power, the *LSM PR* appears over progressively broader ranges of frequency around resonance [(b)-(d)]. The development of *PR* contrast at the hot spot corresponds almost exactly to the deviations of the global $|S_{21}(f)|$ response from the linear/Lorentzian behavior. This demonstrates quite clearly the direct correspondence between hot spot formation and nonlinear response in superconducting resonators.

IV. CONCLUSIONS

In conclusion, we presented experimental evidence linking the global nonlinear microwave transmission characteristics of a superconducting resonator with hot spots induced inside the material making up the resonator. The hot spots are imaged with *LSM* technique at various stages of development and their influence on the global transmission characteristics is documented.

ACKNOWLEDGEMENTS

We gratefully acknowledge the contributions of John Abrahams, Tian Lan, Liza Sarytchev and Brian Straughn. The work at Maryland was supported by ONR Award No. N000140811058 and 20101144225000, the U.S. DOE DESC 0004950, the ONR/UMD AppEl Center, task D10 (N000140911190), and CNAM. The work in Karlsruhe is supported by the Fundamental Researches State Fund of Ukraine and the German BMBF under Grant Project No. UKR08/011 the DFG-Center for Functional Nanostructures (CFN), and a NASU program on “nanostructures, materials and technologies.”

- ¹ I. Siddiqi, R. Vijay, F. Pierre, C. M. Wilson, M. Metcalfe, C. Rigetti, L. Frunzio, and M. H. Devoret, Phys. Rev. Lett. **93**, 207002 (2004).
- ² P. J. Burke, R. J. Schoelkopf, D. E. Prober, A. Sklare, W. R. McGrath, B. Bumble, and H. G. LeDuc, Appl. Phys. Lett. **68**, 3344 (1996).
- ³ B. A. Mazin, D. Sank, S. McHugh, E. A. Lucero, A. Merrill, J. Gao, D. Pappas, D. Moore, and J. Zmuidzinas, Appl. Phys. Lett. **96**, 102504 (2010).
- ⁴ A. Semenov, P. Haas, H. W. Hubers, K. Ilin, M. Siegel, A. Kirste, D. Drung, T. Schurig, and A. Engel, J. Mod. Opt. **56**, 345 (2009).
- ⁵ A. Wallraff, D. Schuster, A. Blais, L. Frunzio, R. Huang, J. Majer, S. Kumar, S. Girvin, and R. Schoelkopf, Nature **431**, 162 (2004); M. A. Sillanpaa, J. I. Park, and R. W. Simmonds, Nature **449**, 438 (2007); R. J. Schoelkopf and S. M. Girvin, Nature **451**, 664 (2008); M. Hofheinz, H. Wang, M.

- Ansmann, Radoslaw C. Bialczak, Erik Lucero, M. Neeley, A. D. O’Connell, D. Sank, J. Wenner, John M. Martinis, and A. N. Cleland, Nature **459**, 546 (2009).
- ⁶ N. Lazarides, and G. P. Tsironis, Appl. Phys. Lett. **90**, 163501 (2007).
- ⁷ C. Kurter, P. Tassin, L. Zhang, Th. Koschny, A. P. Zhuravel, A. V. Ustinov, S. M. Anlage, Costas Soukoulis, Phys. Rev. Lett. (in press) (2011).
- ⁸ H. T. Chen, H. Yang, R. Singh, J. F. O’Hara, A. K. Azad, S. A. Trugman, Q. X. Jia, and A. J. Taylor, Phys. Rev. Lett. **105**, 247402 (2010).
- ⁹ S. M. Anlage, J. Opt. **13**, 024001 (2011).
- ¹⁰ S. M. Anlage, W. Hu, C. P. Vlahacos, D. Steinhauer, B. J. Feenstra, S. K. Dutta, A. Thanawalla, and F. C. Wellstood, J. Supercond. **12**, 353 (1999).
- ¹¹ M. W. Brenner, S. Gopalakrishnan, J. Ku, T. J. McArdule, J. N. Eckstein, N. Shah, P. M. Goldbart, and A.

- Bezryadin, Phys. Rev. B **83**, 184503 (2011); J. Ku, V. Manucharyan, and A. Bezryadin, Phys. Rev. B **82**, 134518 (2010); G. Ghigo, R. Gerbaldo, L. Gozzelino, F. Laviano, and E. Mezzetti, Phys. Rev. B **82**, 054520 (2010).
- ¹² W. J. Skocpol, M. R. Beasley, and M. Tinkham, J. Appl. Phys. **45**, 4054 (1974); G. Hampel, P. Kolodner, P. L. Gammel, P. A. Polakos, E. de Obaldina, P. M. Mankiewich, A. Anderson, R. Slattery, D. Zhang, G. C. Liang, and C. F. Shih, Appl. Phys. Lett. **69**, 571 (1996); M. Tinkham, J. U. Free, C. N. Lau, and N. Markovic, Phys. Rev. B **68**, 134515 (2003); B. Abdo, E. Segev, O. Shtempluck, and E. Buks, Appl. Phys. Lett. **88**, 022508(2006); E. Segev, B. Abdo, O. Shtempluck, and E. Buks, Phys. Lett. A **366**, 160 (2007); N. Shah, D. Pekker, and P. M. Goldbart, Phys. Rev. Lett. **101**, 207001 (2008); E. A. Tholen, A. Ergl, E. M. Doherty, F. M. Weber, F. Grgis, and D. B. Haviland, Appl. Phys. Lett. **90**, 253509 (2007).
- ¹³ C. Kurter, J. Abrahams, and S. M. Anlage, Appl. Phys. Lett. **96**, 253504 (2010).
- ¹⁴ C. Kurter, A. P. Zhuravel, J. Abrahams, C. L. Bennett, A. V. Ustinov, and S. M. Anlage, IEEE Trans. Appl. Supercond. **21**, 709 (2011).
- ¹⁵ B. A. Willemsen, T. Dahm, and D. J. Scalapino, Appl. Phys. Lett. **71**, 3898 (1997).
- ¹⁶ M. Ricci, H. Xu, R. Prozorov, A. P. Zhuravel, A. V. Ustinov, and S. M. Anlage, IEEE Trans. Appl. Supercond. **17**, 918 (2007).
- ¹⁷ A. P. Zhuravel, S. M. Anlage, and A. V. Ustinov, Appl. Phys. Lett. **88**, 212513 (2006).
- ¹⁸ A. P. Zhuravel, A. V. Ustinov, K. S. Harshavardhan, and S. M. Anlage, Appl. Phys. Lett. **81**, 4979 (2002); A. P. Zhuravel, S. M. Anlage, and A. V. Ustinov, J. Supercond. Nov. Mag. **19**, 625 (2006); A. P. Zhuravel, A. G. Sivakov, O. G. Turutanov, A. N. Omelyanchouk, S. M. Anlage, A. Lukashenko, A. V. Ustinov, and D. Abraimov, Low Temp. Phys. **32**, 592 (2006); A. P. Zhuravel, S. M. Anlage, S. K. Remillard, A. V. Lukashenko, and A. V. Ustinov, J. Appl. Phys. **108**, 033928 (2010).
- ¹⁹ The experimental conditions for the measurements presented in Fig. 1 and Fig. 2 are different, so slight changes in resonant frequency and critical power are inevitable.
- ²⁰ R. P. Huebener, *Magnetic Flux Structures in Superconductors* (Springer-Verlag, Berlin, 1979).
- ²¹ V. I. Kuznetsov and V. A. Tulin, JETP Lett. **61**, 1026 (1995).
- ²² A. G. Sivakov, A. P. Zhuravel, I. M. Dimitrenko, V. G. Volotskaya, and O. A. Koretskaya, Sov. Phys.: Superconductivity: Physics, Chemistry and Technology **5**, 1680 (1992).
- ²³ V. M. Dmitriev, I. V. Zolocheskii, and E. V. Khristenko, Low Temp. Phys. **27**, 165 (2001).